

Constraining scalar-tensor theories of gravity from the most massive neutron stars

Carlos Palenzuela¹ and Steven L. Liebling²

¹*Departament de Física, Universitat de les Illes Balears and Institut d'Estudis Espacials de Catalunya, Palma de Mallorca, Balears E-07122, Spain*

²*Department of Physics, Long Island University, Brookville, New York 11548, USA*

(Dated: August 24, 2018)

Scalar-tensor (ST) theories of gravity are natural phenomenological extensions to general relativity. Although these theories are severely constrained both by solar system experiments and by binary pulsar observations, a large set of ST families remain consistent with these observations. Recent work has suggested probing the unconstrained region of the parameter space of ST theories based on the stability properties of highly compact neutron stars. Here, the dynamical evolution of very compact stars in a fully nonlinear code demonstrates that the stars do become unstable and that the instability, in some cases, drives the stars to collapse. We discuss the implications of these results in light of recent observations of the most massive neutron star yet observed. In particular, such observations suggest that such a star would be subject to the instability for a certain regime; its existence therefore supports a bound on the ST parameter space.

PACS numbers: 04.25.-g, 04.25.D-, 04.30.-w

Introduction: Despite the tremendous success of general relativity throughout its first hundred years as a description of gravity, alternative theories remain attractive. Motivated either by purely theoretical ideas such as string theory or more phenomenological issues such as dark matter [1], alternative gravity is severely constrained by observations [2]. One particularly interesting class of theories are the scalar-tensor (ST) theories of gravity in which gravity is mediated by a metric and a scalar field. A primary advantage of ST theories is that they retain a characteristic structure similar to that of GR and are similarly well-posed. Another advantage is that, in an appropriate limit, GR is recovered. Hence, ST theories will always have some parameter region that satisfies the same observational constraints obeyed by GR. Nevertheless, ST theories offer additional degrees of freedom with which to explore phenomena such as dark energy.

If the universe allows for such degrees of freedom, then perhaps we can find observational consequences using the population of observed neutron stars (NS). Here we restrict ourselves to a particular set of ST theories, namely the Damour-Esposito-Farese [3, 4] model which is characterized by two constants, $\{\varphi_0, \beta\}$. The first constant, φ_0 , is the asymptotic value of the scalar field which is constrained by solar system observations to be quite small. The second constant, β , measures the linear, effective coupling between the scalar field and the regular matter content (more detail and the precise form of the action follows below). When both these constants vanish, one recovers GR.

Previous work with neutron stars found for $\beta < -4.5$ that stars underwent spontaneous scalarization in which the scalar field acquired a value in the neighborhood of the star much larger than its asymptotic value φ_0 . As discussed below, scalarization effects lead to constraints on β from below. However, the positive β region remains largely unconstrained, and it is therefore important to

find dynamics in this region with which to compare to observations.

For β above some critical value, β_{crit} , an instability for very compact neutron stars has been found [5]. Although noticed quite some time ago (i.e., see for instance Fig. 5 in Ref. [6] and also in Ref. [7]), it was only recently realized that this instability could appear in the stable branch of equilibrium configurations of realistic microphysical EoS. Although linear perturbation analysis reveals the instability, such an analysis does not indicate the end-state or whether the instability could simply drive the system to a stable configuration. This instability may occur in a wider class of alternative gravity theories, such as $f(R)$ gravity [8] (also see Section IIIA of Ref. [9]), and so similar bounds may be found for other theories.

In order to study this instability and its end state, we perform fully non-linear dynamical evolutions of neutron star solutions with different compactness $C \equiv GM/Rc^2$ until they relax to their final stationary state. For stars with low compactness ($C < 0.27$), the initial data simply relaxes to a ST equilibrium configuration for any value of β . For very compact stars ($C \geq 0.29$) the instability drives the star to collapse to a black hole if β exceeds some critical value, $\beta_{\text{crit}} \approx 90$. For intermediate compactness ($C \approx 0.28$), these two disparate behaviors are also observed, but another behavior, intermediate between collapse and stability, appears. For $\beta > \beta_{\text{crit}}$ but β not too large, the central scalar field grows promptly until the instability saturates and then the solution undergoes damped oscillations about an ST equilibrium solution.

In addition to studying this instability in the fully non-linear regime, we also are able to study non-spherically symmetric stars which allow for rotation. For rotating stars, we find similar behavior of the instability. We discuss the implications of these results in the astrophysical context of very massive neutron stars. The most massive neutron star ever observed has mass $M_{\text{NS}} = 2.01 \pm 0.04 M_{\odot}$ [10] and an estimated radius of roughly

$R_{\text{NS}} \approx 10.5_{-1.0}^{+1.2} \text{km}$ [11]. These values lead to an estimated compactness high enough ($C \approx 0.28$) under most EoS to develop this instability, and therefore the existence of the star suggests an upper bound of $\beta \approx \mathcal{O}(1000)$.

Phenomenological constraints: We consider a general ST theory with action

$$S = \int d^4x \frac{\sqrt{-g}}{2\kappa} \left[\phi R - \frac{\omega(\phi)}{\phi} \partial_\mu \phi \partial^\mu \phi \right] + S_M[g_{\mu\nu}, \psi], \quad (1)$$

where $\kappa = 8\pi G$ (adopting $c = 1$ throughout this paper), R is the Ricci scalar, g is the determinant of the metric, ϕ is the gravitational scalar, and ψ collectively describes the matter degrees of freedom. Although Eq. (1) is not the most general action yielding second-order field equations, it includes a large set of theories by allowing the coupling $\omega(\phi)$ to depend on the scalar fields. Notice that, for simplicity, no potential $V(\phi)$ is included here.

One can re-express the (“Jordan-frame”) action (1) in the so-called “Einstein-frame” through a conformal transformation $g_{\mu\nu}^E = \phi g_{\mu\nu}$, which yields

$$S = \int d^4x \sqrt{-g^E} \left(\frac{R^E}{2\kappa} - \frac{1}{2} g_E^{\mu\nu} \partial_\mu \varphi \partial_\nu \varphi \right) + S_M \left[\frac{g_{\mu\nu}^E}{\phi(\varphi)}, \psi \right] \quad (2)$$

where this scalar field, φ , is defined in terms of ϕ by $(d \log \phi / d\varphi)^2 \equiv 2\kappa / [3 + 2\omega(\phi)]$. A common feature of these families of ST theories is the absence of a direct coupling between the matter degrees of freedom and the scalar field, since otherwise there would be a scalar “fifth force” that has not been observed. However, there is an indirect coupling between matter and scalar field mediated by gravity, which can be expanded in Taylor series around the asymptotic “vacuum” value of the scalar field, φ_0 . For instance, the Jordan-Fierz-Brans-Dicke (JFBD) theories are recovered by considering only the first constant term in this expansion, although solar system tests constrain this constant to very small values.

In this work we focus on the Damour and Esposito-Farese (DEF) family of ST theories [3, 4] which are the next most simple family. In DEF theories, the coupling includes up to the term linear in φ in the Taylor series expansion

$$\frac{1}{2} \frac{d \log \phi}{d\varphi} = -(4\pi G) \beta \varphi \quad (3)$$

corresponding to the choice

$$\omega(\phi) = -3/2 - 1/(2\beta \log \phi), \quad \phi = \exp(-4\pi G \beta \varphi^2). \quad (4)$$

The DEF theories, characterized by the coupling constant β and by the asymptotic value of the scalar field φ_0 , have been shown to produce effects differing significantly from GR in strong-field regimes such as the interior of NS [3, 4]. These effects have led to a number of observational constraints. More specifically, if β is sufficiently

negative, the trivial vacuum of the scalar field becomes unstable and it becomes energetically favorable for the scalar field to settle down into a non-trivial configuration inside the NS (“spontaneous scalarization”). This configuration with a large scalar field in the stellar interior affects not only NS mass and its radius, but also its orbital motion if the star is in a binary. This modification to orbital motion arises because scalarization enhances the gravitational attraction between the components of the binary and triggers the emission of dipolar scalar radiation [12–14]. These effects lead to constraints on the nondimensional constant β such that $\beta \gtrsim -4.5$ using binary pulsar data [4, 10, 15, 16] while the Cassini experiment constrains $\varphi_0 < 1.26 \times 10^{-2} G^{1/2} / |\beta|$.

All these results, however, probe the strong-field, mildly relativistic regime since they involve either static/stationary configurations or velocities much smaller than the speed of light (e.g. binary pulsars have velocities $v \approx 10^{-3}c$). Simulations of coalescing binary neutron stars show that large deviations from GR develop at separations much smaller than those observed with binary pulsars, providing signals that are, at least in principle, observable with existing gravitational-wave detectors such as Advanced LIGO/Virgo [17–19].

Much less constrained is the positive regime of β (see e.g. Fig. 7 of Ref. [10]). Indeed, cosmological studies have shown that in the $\beta > 0$ regime ST theory approaches GR exponentially (i.e. GR is an attractor in the theory phase space) and that the parametrized post-Newtonian (PPN) parameters are exponentially close to their GR values [20, 21]. Thus the instability studied in Ref. [5] represents an important opportunity to constrain the positive β regime. A significant observation of Ref. [5] is that the high compactness required by this instability could occur for otherwise stable NS (ie with masses less than the maximum supported by the EoS). Here we therefore evolve high compactness stars within DEF gravity to study nonlinear effects and the ultimate fate of stars subject to this instability.

Equations of Motion: In the Einstein frame the ST field equations are quite similar to the standard Einstein equations minimally coupled to a scalar field but with a coupling between the scalar field and the matter. The full system of equations takes the form

$$G_{\mu\nu}^E = \kappa (T_{\mu\nu}^\varphi + T_{\mu\nu}^E), \quad (5)$$

$$\square^E \varphi = -(4\pi G) \beta \varphi T_E, \quad (6)$$

$$\nabla_\mu^E T_E^{\mu\nu} = (4\pi G) \beta \varphi T_E g_E^{\mu\nu} \partial_\mu \varphi, \quad (7)$$

where

$$T_E^{\mu\nu} = [\rho_E(1 + \epsilon_E) + p_E] u_E^\mu u_E^\nu + p_E g_{\mu\nu}^E \quad \text{and} \quad (8)$$

$$T_{\mu\nu}^\varphi = \partial_\mu \varphi \partial_\nu \varphi - \frac{g_{\mu\nu}^E}{2} g_E^{\alpha\beta} \partial_\alpha \varphi \partial_\beta \varphi \quad (9)$$

are the matter and scalar-field stress-energy tensors in the Einstein frame and $T_E \equiv T_E^{\mu\nu} g_{\mu\nu}^E$. Baryon number

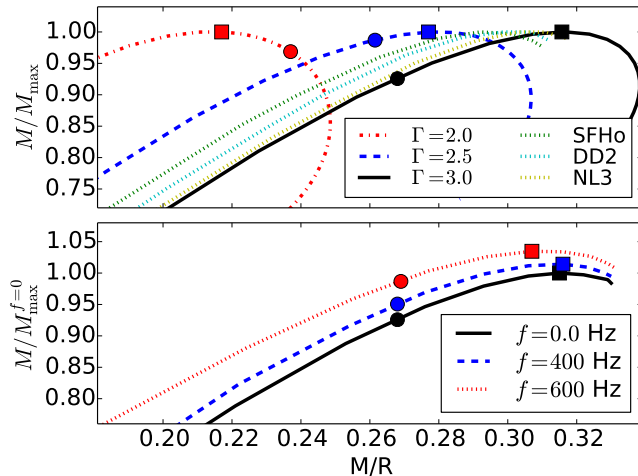


FIG. 1: Characterization of initial stellar models. **Top:** Mass versus compactness of spherical, non-rotating neutron star equilibrium configurations for different polytropic exponent (e.g. stiffness) in the polytropic EoS $p = K\rho^\Gamma$. The transition between models with T everywhere negative to models with T positive in a central region is marked (solid circles) for each value of Γ . The stable branch lies on the left of the maximum of the curve. Solutions for three microphysical EoS are also included, showing that their structure lies between that of the polytropes with $\Gamma = 2.5$ and $\Gamma = 3$. **Bottom:** Mass versus compactness for rigidly rotating neutron stars with fixed $\Gamma = 3$ but different rotational frequencies. Notice that the transition in T lies at roughly the same compactness as for the nonrotating models. However, as the frequency increases, the configuration at the transition has a mass closer to the maximum mass than the nonrotating case. Again, the stable branch lies on the left of the maximum mass.

conservation in the Jordan frame leads to

$$\nabla_\mu^E j_E^\mu = (4\pi G)\beta\varphi j_E^\mu \partial_\mu \varphi, \quad (10)$$

with $j_E^\mu = \rho_E u_E^\mu$. In other words, neither the current associated with baryon number nor the stress-energy tensor are generally conserved in the Einstein frame and instead has source terms. Solving the system (5), (6), (7) and (10) and transforming back to the Jordan frame provides a solution to the original problem.

Initial data: We construct the initial data for our neutron stars as follows. We begin by solving for a stellar configuration that is at equilibrium in GR as described below. In addition, we specify the initial scalar field as a constant, $\varphi(x^i, t = 0) = \varphi_0$.

It is straightforward to show that these initial data are also solutions to ST theory in the Einstein frame. In particular, the stress-energy tensor of the scalar field, $T_{\mu\nu}^\varphi$, given by Eq. (9) is initially zero when φ is constant, and hence Eq. (5) is satisfied by the GR solution. The fluid equations in Eq. (7) are also satisfied by a constant scalar field. Although the initial data is a solution within ST theory, the scalar field is sourced via Eq. (6) and hence

is no longer in equilibrium. Instead, the initial data is at a moment of time symmetry with an initial “acceleration.”

These solutions represent perturbed stellar configurations, and this same procedure is adopted both by Refs. [5] and [6] in their linear perturbation analysis. In this case, the magnitude of the perturbation depends, in part, on the value of β . Indeed, one could imagine a scenario in which such a perturbed star might result naturally. In particular, consider a neutron star with small compactness, so that the star begins with a small, nearly constant scalar field in its interior. The compactness might increase suddenly by going supernova, accreting mass, or undergoing a merger, while maintaining a fairly constant and small scalar field.

We use the LORENE code [22] to construct the initial stellar models. The stars are described by a polytropic equation of state, $p/c^2 = K\rho_0^\Gamma$, which is a reasonable approximation for cold stars. In our search for solutions subject to the instability, we explore a range of values of the adiabatic index $\Gamma = 2 - 3$, but only $\Gamma = 3$ is chosen for our evolutions. The choice here of K is not important since the solution can be rescaled to match the maximum mass $M \approx 2.0M_\odot$ of the most massive observed neutron star [10].

We focus on configurations fulfilling two conditions: (i) lying on the stable branch of solutions and (ii) having compactness sufficient to achieve a region with $T > 0$ in its central interior (in contrast, stars generally have $T < 0$ everywhere). This second condition is crucial for the existence of the instability, and we have verified that no instability is apparent for configurations which lack such a region. Notice that the positivity of the trace is independent of the frame because $T = \phi^2 T_E$. In the case of the perfect fluid described by Eq. (8), the trace can be written as

$$T = 3p - \rho(1 + \epsilon) = \left(\frac{3\Gamma - 4}{\Gamma - 1}\right)p - \rho = \left(\frac{3\Gamma - 4}{\Gamma - 1}\right)K\rho^\Gamma - \rho \quad (11)$$

where the first equality is completely generic and in the second we have used the ideal gas EoS law, $p = (\Gamma - 1)\rho\epsilon$. The third equality uses a polytropic relation for the pressure which only applies to isentropic fluids without shocks.

We characterize a range of these solutions in Fig. 1. The mass of nonrotating solutions is shown in the top panel of Fig. 1 as a function of compactness. Where the maximum mass is achieved represents a turning point (marked with a square) in stability such that solutions of smaller compactness are stable (in GR) whereas more compact solutions are unstable. Three families of solutions, each with a different EoS parameter Γ , are shown, and it is apparent that larger values correspond to more compact stars.

As these stars get more compact, the solutions eventually reach a point where T becomes positive in their interior. The point at which solutions achieve $T = 0$ is marked with a circle so that more compact stars have regions with positive trace. It is important to note that for

small Γ , the circle is to the right of the square whereas for large Γ one has the opposite. This note is important because, for $\Gamma = 3$ for example, one has solutions on the stable branch that nevertheless have regions of positive trace. It is precisely the evolution of these solutions that is of interest here. Interestingly, the null point seems mostly independent of the value of Γ , lying at a compactness of $C \approx 0.27$. Indeed, the results of Ref. [5] with realistic EoS also find similarly high compactness solutions on the stable branch. We include the family of curves of other realistic EoS in Fig. 1 showing that these EoS have solutions similar to that of $\Gamma = 3$ despite spanning a wide range of stiffness (e.g. resulting radii).

A similar plot but instead for rigidly rotating solutions is shown in the bottom panel of Fig. 1. Here, instead of different values of Γ , solutions rotating at different frequencies, f , are shown, all for $\Gamma = 3$. As before, the separation between stability branches is marked with a square and the null point where T changes sign is marked with a circle. Notice that the null point is roughly at the same compactness $C \approx 0.27$ for any frequency.

Numerical simulations: Our numerical code for evolving these configurations has been described and tested previously [23, 24] finding a dynamical scalarization effect in the evolution of binary NS systems in ST [17, 18]. The initial data are evolved on a cubical computational domain $x^i \in [-160, 160]$ employing fixed mesh refinement with a finest grid spacing $\Delta x = R_{\text{NS}}/50$. Certain evolutions were conducted at higher resolutions up to $\Delta x = R_{\text{NS}}/70$ to verify convergence. We vary the effective coupling by considering different values of β (i.e., keeping $\varphi_0 \leq 10^{-5} G^{-1/2}$ fixed). We have checked that the results do not change significantly when φ_0 is varied within those bounds.

We employ an ideal gas EoS for our simulations choosing $\Gamma = 3$ so that solutions containing $T > 0$ lie on the stable branch in GR. We evolve initial data along this family parametrized by the compactness.

We begin by discussing our evolutions of a configuration with compactness $C = 0.26$. For this initial data, the trace is everywhere negative and no instability is expected. Indeed, in our evolutions we increased β up to a value of 8000 with no indication of instability. In particular, the central density and lapse remained unchanged with increasing β . The scalar field demonstrated fast oscillations with an amplitude damped in time. For very large values of β , the overall amplitude was diminished.

In stark contrast, the evolution of a high compactness configuration ($C = 0.29$) is shown in Fig. 2. These evolutions display two disparate behaviors depending on the value of β . For $\beta > \beta_{\text{crit}}$ (here $\beta_{\text{crit}} \approx 90$), the central density and scalar field grow more than an order of magnitude while the star collapses to a black hole. For $\beta < \beta_{\text{crit}}$, these quantities oscillate (but with a slow drift that decreases with increasing resolution). In particular, the density slowly increases by a few percent while the lapse decreases by an even smaller amount. The scalar

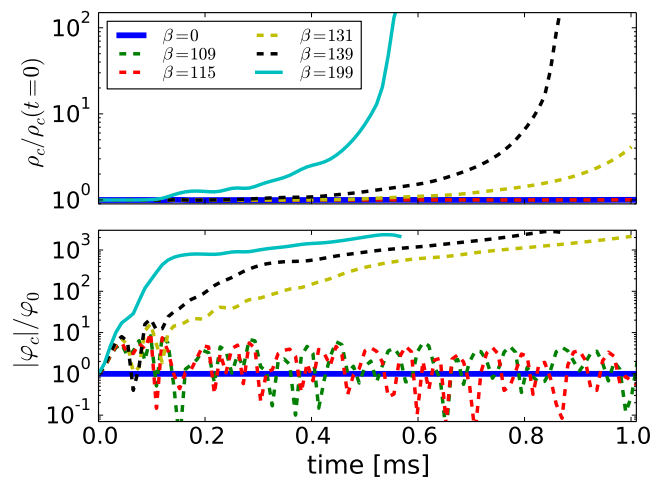


FIG. 2: *Dynamics of a highly compact ($C = 0.29$), non-rotating star. **Top:** Central value of the rest-mass density, ρ_c , as a function of time. **Bottom:** Central value of the scalar field, φ_c . Note that the $\beta = 0$ solution is stable whereas the scalar field grows initially for nonvanishing β . However, only for $\beta > \beta_{\text{crit}}$ does the central density grow apparently without bound, collapsing to a black hole. For $\beta < \beta_{\text{crit}}$, the scalar field oscillates, sometimes transitioning to negative values. Here $\beta_{\text{crit}} \approx 90 \pm 10$ with the uncertainty arising due to late time instability.*

field oscillates about either zero or its initial value.

These evolutions suggest that for small β , the configurations evolve to a stable, ST equilibrium solution. Because the scalar field is the most dynamic aspect of the solution in this regime, we plot it for a few times as it settles to its final state in Fig. 3. Included in the figure is the corresponding static star found by integrating the analogous TOV-like system of equations. The evolution approaches the static star oscillating with a damped amplitude within the central region.

For larger β , the instability drives the evolution to collapse. As one decreases β and approaches β_{crit} from above, the growth of the central density is delayed further in time. One can estimate the survival time of the configuration by choosing a large, fiducial value of the scalar field and measuring the time it takes the central scalar field to reach this value. This fiducial time t_f is plotted as a function of β in Fig. 4. It is notable that both spherical and rotating solutions (with frequency 400Hz) appear to demonstrate the same scaling, namely that $t_f \propto |\beta - \beta_{\text{crit}}|^{-0.65}$, and that the scaling exponent, -0.65 , is roughly comparable to the approximate value -0.5 presented in Ref. [6] [see Eq. (5.3)].

For $C = 0.28$ we find an intermediate regime in β . For such cases, we see the growth of the instability in the center of the star. However, this growth ceases after which the central region oscillates with an exponentially decreasing amplitude. The solution appears to settle to its corresponding ST equilibrium solution. The difference between this case and the small β cases would appear to

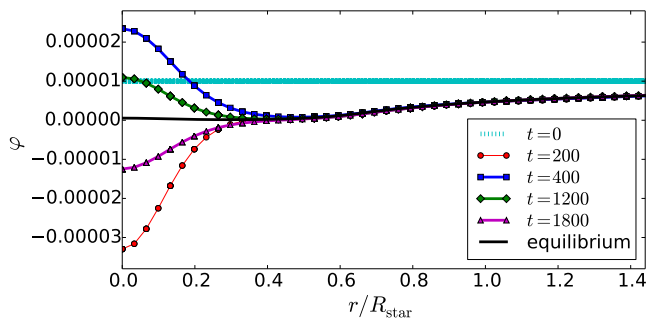


FIG. 3: Evolution of the scalar field for a highly compact ($C = 0.29$), non-rotating star with $\beta = 80$. The scalar field as a function of radius at different times during the evolution is shown. Also shown is the equilibrium configuration (solid black) within ST with the same central density as the initial data. At late times the solution relaxes to the equilibrium configuration with a slowly damped, oscillating central region.

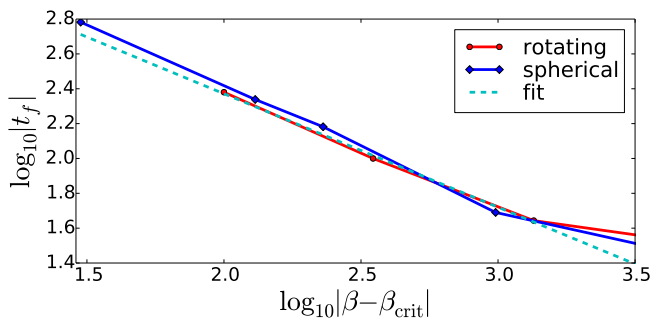


FIG. 4: Growth rate for highly compact ($C = 0.29$) stars. To determine the growth rate of the instability as a function of β , the time, t_f , is found at which the scalar field at the center has increased by a factor of 600 (an arbitrary, fiducial value). This fiducial time appears to scale as $t_f \propto |\beta - \beta_{\text{crit}}|^\gamma$ with $\gamma \approx -0.65$ (cyan, dashed) for both non-rotating, spherical stars (blue, solid) and rotating stars (red, solid).

be the initial instability in the central region. The oscillations in this region propagate via the scalar degree of freedom to large radius. The nature of the transition from this intermediate regime to the collapsing regime and the question of whether this intermediate regime occurs in the rotating case require further investigation.

Conclusions Our simulations of the fully nonlinear system find that very compact stars containing a central region with $T > 0$ become unstable for sufficiently large β , consistent with the linear perturbation results. This instability, studied in detail in [5] in spherical symmetry for different microphysical EoS, appears for values of $\beta_{\text{crit}} \approx 140$ for a compactness of $C = 0.283$. However, our evolutions show that prompt collapse occurs for $\beta > 700$, and so establishing constraints from observational data may require fully nonlinear solutions. Fig. 5 displays this difference by showing the values of

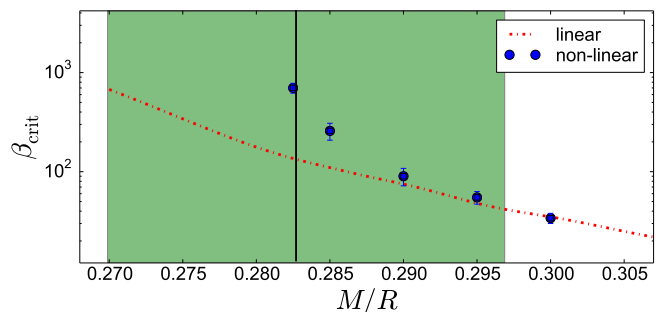


FIG. 5: Stability region as a function of compactness for non-rotating solutions. The value of β at which our numerical evolutions collapse to black hole are shown (blue dots) along with a rough estimate of its uncertainty. The results from the ENG case of Ref. [5] (because of the similarity of that case with the $\Gamma = 3$ case) are also shown (red dotted curve) for comparison. A vertical line (black solid line) indicates the compactness of the most massive star observed assuming a radius of 10.5km [11]. The shaded region (green) around that vertical line indicates the uncertainty in radius (i.e., assuming half of the maximum error) leading to a range of 10 – 11km.

β for which the neutron star undergoes prompt collapse together with the β_{crit} obtained from the linear analysis. In addition, our evolutions extend to rotating solutions which break spherical symmetry and which also demonstrate this same instability.

An important question left unanswered by the perturbation analysis concerns the end-state of the instability. Our evolutions find that these compact stars are driven either to apparently stable ST equilibrium configurations with non-constant profiles for the scalar field or to black hole formation (see Fig. 6). In particular, we conjecture that when starting with a GR solution of some particular mass that it will be driven to a ST solution if such a solution on the stable branch exists with roughly the same mass (or a bit less). However, for large β , such an approach to stable solutions is more difficult since the maximum mass gets smaller as β increases (see, e.g., Fig. 4 of Ref. [5]).

There are at least a couple of different ways of considering the astrophysical implications of this instability. Consider the most massive neutron star ever observed, which has mass $M_{\text{NS}} = 2.01 \pm 0.04 M_\odot$ [10]. To compute its compactness, consider different estimates which favor a radius for neutron stars of roughly $R_{\text{NS}} \approx 10.5^{+1.2}_{-1.0}$ km [11] (see also [25]) for this mass, which would indicate a compactness of 0.283 ± 0.030 . Such a value places it within the unstable regime, but we acknowledge a number of uncertainties. In particular, the uncertainty in the compactness is quite large. Significant uncertainty arises from our ignorance about the appropriate stellar EoS. Additionally, very long evolutions of some cases eventually collapse, and ensuring that the finite boundary is not affecting the solution is difficult. Such a computational difficulty leads to uncertainty in the precise value of β_{crit} .

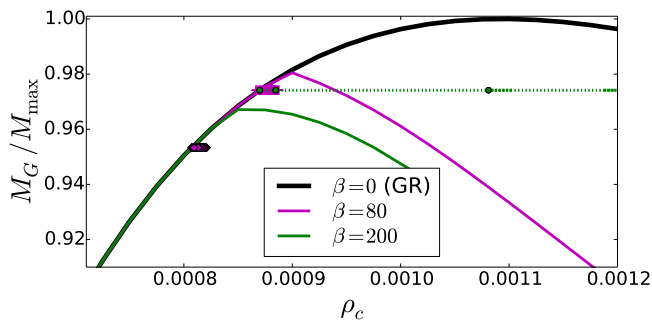


FIG. 6: *Sketch of the configuration space.* Three curves show families of equilibrium solutions for $\beta = 0$ (GR), $\beta = 80$, and $\beta = 200$. Two GR solutions are shown representing the initial data used (along with an initially constant scalar field). The evolution of a low compactness star (the lower solution) shows that the solution oscillates about the nearly identical ST solution, regardless of β . In contrast, the very compact star (with larger central density) has two very different outcomes. For $\beta = 80$, the evolution oscillates about the ST solution (magenta). For $\beta = 200$, however, the evolution (green dashed) proceeds to the right and the solution collapses without approaching any equilibrium solutions.

Perhaps, if gravity is described by DEF ST gravity, the existence of this extreme star argues for an upper limit on

β . If β were higher, such a star might become unstable to collapse. Of course, a precise value of our β awaits more detailed knowledge of the star, but very likely β would be bounded from above by $\beta_{\text{crit}} \approx \mathcal{O}(1000)$.

However, another interpretation, equivalent to that above, is that the maximum observed NS mass is not set by the maximum supported by the particular EoS describing neutron star matter. Instead, the maximum mass may be set by the onset of this instability in ST gravity (or in related, alternative theories such as $f(R)$ gravity [8]). Future observations of massive neutron stars may elucidate this ambiguity and allow for more stringent constraints.

Acknowledgments: We thank Enrico Barausse, Raissa Mendes, and Paolo Pani for helpful discussions. We also acknowledge the support and hospitality of the Fields Institute during their focus program *100 Years of General Relativity* where this work began. This work was supported by the NSF under grant PHY-1308621 (LIU) and by NASA’s ATP program through grant NNX13AH01G. CP acknowledges support from the Spanish Ministry of Education and Science through a Ramon y Cajal grant and from the Spanish Ministry of Economy and Competitiveness grant FPA2013-41042-P. Computations were performed at XSEDE, Scinet, and MareNostrum.

-
- [1] R. Brito, V. Cardoso, and H. Okawa, “Accretion of dark matter by stars,” [arXiv:1508.04773 \[gr-qc\]](#).
- [2] C. M. Will, “The Confrontation between General Relativity and Experiment,” *Living Reviews in Relativity* **17** (June, 2014) 4, [arXiv:1403.7377 \[gr-qc\]](#).
- [3] T. Damour and G. Esposito-Farese, “Nonperturbative strong-field effects in tensor-scalar theories of gravitation,” *Physical Review Letters* **70** (Apr., 1993) 2220–2223.
- [4] T. Damour and G. Esposito-Farèse, “Tensor-scalar gravity and binary-pulsar experiments,” *Phys. Rev. D* **54** (July, 1996) 1474–1491, [gr-qc/9602056](#).
- [5] R. F. P. Mendes, “Possibility of setting a new constraint to scalar-tensor theories,” *Phys. Rev. D* **91** no. 6, (Mar., 2015) 064024, [arXiv:1412.6789 \[gr-qc\]](#).
- [6] T. Harada, “Stability Analysis of Spherically Symmetric Star in Scalar-Tensor Theories of Gravity,” *Progress of Theoretical Physics* **98** (Aug., 1997) 359–379, [gr-qc/9706014](#).
- [7] P. Pani, V. Cardoso, E. Berti, J. Read, and M. Salgado, “Vacuum revealed: The final state of vacuum instabilities in compact stars,” *Phys. Rev. D* **83** no. 8, (Apr., 2011) 081501, [arXiv:1012.1343 \[gr-qc\]](#).
- [8] S. Capozziello, M. De Laurentis, R. Farinelli, and S. D. Odintsov, “The Mass-Radius relation for Neutron Stars in $f(R)$ gravity,” [arXiv:1509.04163 \[gr-qc\]](#).
- [9] T. P. Sotiriou and V. Faraoni, “ $f(R)$ Theories Of Gravity,” *Rev. Mod. Phys.* **82** (2010) 451–497, [arXiv:0805.1726 \[gr-qc\]](#).
- [10] J. Antoniadis, P. C. C. Freire, N. Wex, T. M. Tauris, R. S. Lynch, M. H. van Kerkwijk, M. Kramer, C. Bassa, V. S. Dhillon, T. Driebe, J. W. T. Hessels, V. M. Kaspi, V. I. Kondratiev, N. Langer, T. R. Marsh, M. A. McLaughlin, T. T. Pennucci, S. M. Ransom, I. H. Stairs, J. van Leeuwen, J. P. W. Verbiest, and D. G. Whelan, “A Massive Pulsar in a Compact Relativistic Binary,” *Science* **340** (Apr., 2013) 448, [arXiv:1304.6875 \[astro-ph.HE\]](#).
- [11] F. Ozel, D. Psaltis, T. Guver, G. Baym, C. Heinke, and S. Guillot, “The Dense Matter Equation of State from Neutron Star Radius and Mass Measurements,” *ArXiv e-prints* (May, 2015) , [arXiv:1505.05155 \[astro-ph.HE\]](#).
- [12] D. M. Eardley, “Observable effects of a scalar gravitational field in a binary pulsar,” *Astrophys. J. Lett.* **196** (Mar., 1975) L59–L62.
- [13] T. Damour and G. Esposito-Farese, “Tensor-multi-scalar theories of gravitation,” *Classical and Quantum Gravity* **9** (Sept., 1992) 2093–2176.
- [14] C. M. Will and H. W. Zaglauer, “Gravitational radiation, close binary systems, and the Brans-Dicke theory of gravity,” *Astrophys. J.* **346** (Nov., 1989) 366–377.
- [15] T. Damour and G. Esposito-Farèse, “Gravitational-wave versus binary-pulsar tests of strong-field gravity,” *Phys. Rev. D* **58** no. 4, (Aug., 1998) 042001, [gr-qc/9803031](#).
- [16] P. C. C. Freire, N. Wex, G. Esposito-Farèse, J. P. W. Verbiest, M. Bailes, B. A. Jacoby, M. Kramer, I. H. Stairs, J. Antoniadis, and G. H. Janssen, “The

- relativistic pulsar-white dwarf binary PSR J1738+0333 - II. The most stringent test of scalar-tensor gravity,” *Mon. Not. Roy. Astron. Soc.* **423** (July, 2012) 3328–3343, [arXiv:1205.1450](#) [astro-ph.GA].
- [17] E. Barausse, C. Palenzuela, M. Ponce, and L. Lehner, “Neutron-star mergers in scalar-tensor theories of gravity,” *Phys. Rev. D* **87** no. 8, (Apr., 2013) 081506, [arXiv:1212.5053](#) [gr-qc].
- [18] C. Palenzuela, E. Barausse, M. Ponce, and L. Lehner, “Dynamical scalarization of neutron stars in scalar-tensor gravity theories,” *Phys. Rev. D* **89** no. 4, (Feb., 2014) 044024, [arXiv:1310.4481](#) [gr-qc].
- [19] M. Shibata, K. Taniguchi, H. Okawa, and A. Buonanno, “Coalescence of binary neutron stars in a scalar-tensor theory of gravity,” *Phys. Rev. D* **89** no. 8, (Apr., 2014) 084005, [arXiv:1310.0627](#) [gr-qc].
- [20] T. Damour and K. Nordtvedt, “General relativity as a cosmological attractor of tensor-scalar theories,” *Phys. Rev. Lett.* **70** (Apr, 1993) 2217–2219. <http://link.aps.org/doi/10.1103/PhysRevLett.70.2217>.
- [21] T. Damour and K. Nordtvedt, “Tensor-scalar cosmological models and their relaxation toward general relativity,” *Phys. Rev. D* **48** (Oct, 1993) 3436–3450. <http://link.aps.org/doi/10.1103/PhysRevD.48.3436>.
- [22] LORENE. home page <http://www.lorene.obspm.fr/>, 2010.
- [23] C. Palenzuela, I. Olabarrieta, L. Lehner, and S. L. Liebling, “Head-on collisions of boson stars,” *Phys. Rev. D* **75** no. 6, (Mar., 2007) 064005, [gr-qc/0612067](#).
- [24] M. Anderson, E. W. Hirschmann, L. Lehner, S. L. Liebling, P. M. Motl, D. Neilsen, C. Palenzuela, and J. E. Tohline, “Simulating binary neutron stars: Dynamics and gravitational waves,” *Phys. Rev. D* **77** no. 2, (Jan., 2008) 024006, [arXiv:0708.2720](#) [gr-qc].
- [25] W.-C. Chen and J. Piekarewicz, “On the compactness of neutron stars,” *ArXiv e-prints* (May, 2015) , [arXiv:1505.07436](#) [nucl-th].